Crystal Structure and Characterization of Ag Nanoparticles Synthesized by Microwave-assisted Liquid-phase Reduction

Yuping Xu*, Eiji Nishio**, Yunzi Xin*, Takashi Shirai*, **

* Advanced Ceramics Research Center, Nagoya Institute of Technology, Gokiso-cho, Showa-ku, Nagoya, Aichi 466-8555, JAPAN

** Department of Life Science and Applied Chemistry, Graduate School of Engineering, Nagoya Institute of Technology Gokiso-cho, Showa-ku, Nagoya, Aichi 466-8555, JAPAN

Abstract: The synthesis of metal nanoparticles (NPs) through microwave-assisted liquid-phase reduction has garnered significant attention due to its efficiency in terms of yield, reaction time, and energy consumption, leading to extensive research. Herein, silver (Ag) NPs are synthesized by the microwave liquid-phase reduction method under various heating rates and evaluated the resultant changes in particle size and crystalline structure based on a detailed investigation. The results reveal that higher heating rates during synthesis lead to smaller particle sizes and narrower size distributions, while lower heating rates result in larger particle sizes and broader size distributions. Moreover, our investigation demonstrates that a considerable portion of the Ag NPs obtained through microwave-assisted liquid-phase reduction exhibit a metastable 4H structure rather than the more stable fcc structure found in bulk materials. In addition, the ratio of single crystals to polycrystals, likely affecting the activity of the particle surface, was investigated, in which the higher proportion of polycrystals are observed for Ag NPs synthesized at higher heating rates. We elucidate that at slow heating rate condition, there is a lot of reducing agent, which is gradually supplied to the metal ions and slowly reduced, resulting in the growth of single crystals. Furthermore, we also developed a high-performance catalyst for decomposition of volatile organic compounds by loading Ag NPs on hydroxyapatite. Ag NPs synthesized by microwave-assisted liquid-phase reduction show excellent activity at low temperatures range. The excellent catalytic activity of Ag NPs originating from the unique surface/interface structure tailored by microwave-assisted fast heating is elucidated.

Keywords: Microwave, silver nanoparticles, polyol reduction, crystal structure, catalysis

Introduction

Metal nanoparticles (NPs) have garnered significant interest due to their distinct chemical and physical properties, that render them promising candidates for versatile applications in microelectronics, catalysis, fuel cells, materials science, biotechnology, and medicine.[1-3] Several approaches such as chemical reduction, photochemical reduction, electrochemical reduction, laser ablation, physical vapor deposition, sputtering and arc/spark discharge are commonly employed for the metal NPs preparation, which can be categorized into two main types as bottom-up and top-down methods depending on starting material of NPs preparation.[4-7] Among them, bottom-up liquid-phase synthesis methods stand out for the preparation of metal NPs due to their possibility of precisely controlling the structure, morphology, and chemical properties of resulting nanomaterials.[8-10] One of the most promising methods towards this end is the liquid-phase synthesis of metal NPs utilizing microwave heating.[11-14] This method offers advantages such as accelerated reaction rates, a wider range of heating conditions, and reduced environmental impact compared to conventional heating methods. Within the framework of microwave-assisted liquid-phase synthesis of metal particles, polyol reactions occur in the liquid phase.[15] The polyol reaction, a process involving the reduction of metal ions by polyhydric alcohols in solvent, is instrumental in this method. Notably, ethylene glycol and 1,2-dioal, renowned for their high boiling point and high dielectric constants, enabling sufficient microwave absorption and chemical reaction at relatively high temperatures, are frequently employed as the polyhydric alcohol here.[16]

Silver (Ag) NPs generally hold considerable significance in the field of nanotechnology and materials science due to their unique properties and versatile applications.[17-19] Microwave-assisted synthesis of Ag NPs via liquid-phase polyol reduction has garnered significant attention.[20-22] However, most of the reports, primarily focus on the effects of polyol reducing agents

on the morphology, size, and properties of the final product, largely overlooking the roles of microwave radiation. Ider et al.[23] explored the effects of latex concentration and microwave irradiation time on the morphology, size distribution, and yield of Ag NPs. By introducing a solid intermediate solution mixing step, Julio et al.[24] modified the traditional polyol method and succeeded in improving the efficiency and reaction rate of Ag NPs synthesis. Notably, there is a noticeable gap in research concerning in the effect of precursor reduction dynamics on metal NPs growth and crystallinity formation via liquid-phase polyol reduction utilizing microwave techniques particularly under controlled heating rates. Our previous studies reveal that precursor reduction plays an important role in deciding the crystallinity of platinum (Pt) NPs core-state, that is polycrystalline Pt NPs with twinned crystal planes in microwave-assisted fast heating, and single crystalline Pt NPs in microwave-assisted slow heating. Moreover, the synthesized Pt NPs with a selectively controlled crystal structure, prepared via microwave fast synthesis, exhibits superior catalytic activity for the oxidative decomposition of volatile organic compounds (VOC) when it loaded on hydroxyapatite (HAp).[14] Therefore, it is of significant interest to material design of the catalyst through precise structure control of the noble-metal NPs.

For Ag particles, the fcc structure has high thermal stability and is usually found in nanorods and nanowires, while the 4H structure is a metastable structure.[25] It has been reported that differences in crystal structure effect the decomposition rate of metal NPs as decomposition catalysts. It has been confirmed that ruthenium exhibits higher electrocatalytic activity when both 4H and fcc structures exist.[26] In this study, we focus on the microwave-assisted polyol synthesis of Ag NPs through a detailed investigation of the crystal size and structure, which is effected by microwave irradiation particularly under controlled heating rates. We successfully synthesized Ag NPs with fcc and 4H phases by adjusting microwave conditions, which was unprecedented previously. In addition, we also developed a superior catalyst for VOC elimination by loading the synthesized Ag NPs on HAp. Despite the trace loading amount of Ag NPs in the present work, the developed Ag NPs@HAp exhibited sufficient catalytic activity in the oxidative decomposition of VOC at low temperatures of 200, 300, and 400 ℃.

Experimental method

Synthesis of Ag NPs via microwave-assisted liquid-phase polyol reaction

Silver nitrate ($AgNO_3$, FUJIFILM Wako Pure Chemical Corp. Japan) was used as a precursor, polyvinylpyrrolidone (PVP, mol wt. 10,000, Sigma-Aldrich Co. LLC) as a capping agent, and ethylene glycol ($C_2H_6O_2$, FUJIFILM Wako Pure Chemical Corp. Japan) as a reducing agent. An ethylene glycol solution containing 10 mM silver nitrate and an ethylene glycol solution containing 3 wt% PVP were prepared in an Ar-filled glovebox. A mixture of these two solutions at a volume ratio of 1:1 was used as the starting solution. Synthesis of Ag NPs was carried out under the conditions of setting the reaching temperature and heating rate in the microwave-irradiation equipment (Discover 2.0, CEM Corp.). Ag NPs were synthesized under the conditions in which the reaching temperature was set to 160 ℃ where the polyol reaction was confirmed, and the heating rate was set to 65, 41, 6.5, 4.1, 3.3, 2.6, 2.2 ℃/min. Microwave irradiation was immediately stopped once the target temperature was reached, and the product was cooled naturally to room temperature (<30 ℃).

Characterizations of synthesized Ag NPs

The UV-vis absorption of the Ag NP solutions was analyzed by a UV-vis spectrometer (V-750, JASCO Corp. Japan). The size distribution of Ag NPs in ethylene glycol was confirmed by dynamic light scattering (DLS) using commercial equipment (Zetasizer, Malvern Panalytical Ltd. UK). The size, morphology, and crystallinity of Ag NPs in solid state were evaluated using high-resolution transmission electron microscopy (HR-TEM, JEM-ARM200, JEOL Ltd. Japan). For the HR-TEM sample preparation, a drop of ethanol solution of Ag NPs obtained by the following purification procedure was dropped onto the carbon support film and vacuum dried in 1 day for observation. The purification process involves adding 5 ml of ethylene glycol solution containing Ag NPs to 25 ml of acetone, followed by centrifugation in a commercial apparatus to precipitate the Ag NPs. After three rounds of separation and washing, the Ag NPs were vacuum dried overnight. Subsequently, 2.5 ml of ethanol (C_2H_6O, FUJIFILM Wako Pure Chemical Corp. Japan) was added to disperse the purified Ag NPs. The surface charge of Ag NPs at different pH levels was measured by zeta potential analysis using a commercial

instrument (Zetasizer, Malvern Panalytical Ltd. UK).

Fabrication of Ag NPs loaded on HAp (Ag NPs@HAp) Composite

This work was conducted based on a reported manner.[14] The commercial HAp powder (Taihei Chemical Corp. Japan) featuring a chemical composition of Ca/P = 1.70 and an average particle size of 50 nm was utilized. To obtain a well-dispersed HAp slurry with a solid loading amount of 10 vol%, a wet-jet milling system (Star Burst Mini HJP- 25001CE, Sugino Co., Ltd. Japan) was employed. The Ag NPs@HAp composite was prepared through electrostatic adsorption by mixing an aqueous slurry of HAp and an aqueous dispersion of Ag NPs. During this process, the surface charge of HAp was adjusted by adding poly(diallyldimethylammonium chloride) (PDDA) as a surface functionalization agent to facilitate optimal binding with Ag NPs. The combination of HAp and Ag NPs was achieved using 1 wt% PDDA at pH = 7.0. Subsequently, the prepared Ag NPs@HAp composite was separated from water via high-speed centrifugation at 10,000 rpm for 10 min. The resultant Ag NPs@HAp powder was collected after freeze-drying for 48 h, followed by calcination at 600 ℃ for 2 h to remove organic components. The exact loading amount of Ag NPs in the composite was estimated by inductivity coupled plasma optical emission spectrometry (ICP-OES, ICPE-9820, Shimadzu Corp. Japan).

Catalytic test for VOC decomposition of Ag NPs@HAp composite

To evaluate the catalytic activity for oxidative decomposition of VOCs, ethyl acetate was used at a concentration of 100 ppm and mixed with pure air at a volume ratio of 1:1. Then the gas flowed on 1 g of Ag NPs@HAp powder at a speed of 0.25 L/min. The decomposition gases collected at 100, 200, 300, and 400 ℃ were analyzed by gas chromatography flame ionization detector (GC-FID, GC2030, Shimadzu Corp Japan) and CO_2 concentration was measured by an infrared gas analyzer (CGT-7100, shimadzu Corp. Japan). The conversion, CO_2 selectivity, and inorganic conversion were calculated by equations described in our previous reports.[8]

Results and discussion

The Ag NPs produced in this experiment were confirmed by UV-vis absorbance. The absorption peaks of the Ag NPs were identified, and the results are shown in Figure 1 (a). The peak observed at 200~250 nm comprises a combination of Ag ion and PVP peaks, whereas the peak at 400~420 nm is attributed to the surface plasmon resonance of Ag NPs.[27] The shift of the peak towards longer wavelengths as slower heating rate is a consequence of increased NPs size. The peak of surface plasmon resonance varies based on the shape and concentration of NPs.[28] However, as depicted in the subsequent HR-TEM observation, the shape remains consistent across all samples, suggesting a higher concentration of Ag NPs synthesized under slower heating rates. This can be attributed to the prolonged heating since NPs formation. Figure 1(b) illustrates the hydrodynamic size of the obtained Ag in ethylene glycol solution under different heating rates. This result indicates that Ag NPs synthesized by microwave under slower heating rates exhibit larger sizes. This conclusion is consistent with the result of UV-vis, that is, the rapid heating produced smaller particles than those produced under slow heating processes.

The HR-TEM images reveal the morphologies and size of Ag NPs synthesized via microwave-assisted heating under different heating rates. As shown in Figure 2(a-g), the Ag NPs with a spherical shape of 30 nm or smaller have been synthesized under all conditions. In addition, Ag NPs synthesized under slower heating rates exhibit larger particle sizes and broader size distributions. This phenomenon arises because slower heating rates lead to longer microwave irradiation times and accelerated particle growth. Figure 2(h) shows the HR-TEM image focusing on the crystalline structure of Ag NPs and the assessment of lattice spacing. The upper panel in Figure 2(h) displays a lattice spacing of 0.250 nm, indicating the (100) plane of the 4H structure, which is a metastable structure of Ag NPs.[29] While the lower panel exhibits a lattice spacing of 0.231 nm, indicating the (111) plane of the fcc structure of Ag NPs.[30] Interestingly, across all synthesized Ag NPs at different heating rates in this study, the 4H structure was more prevalent than the fcc structure. However, the fcc structure of Ag in bulk is known to be the most stable in the absence of surface effects, the situation differs for NPs due to the significant surface effects. Indeed, the existence of 4H structure has been confirmed in nanostructured Ag and suggests that as the size of Ag nanowires increases, the proportion of 4H structures decreases.[31] Therefore, a similar trend can be expected to occur for Ag NPs as a function of size, interplay

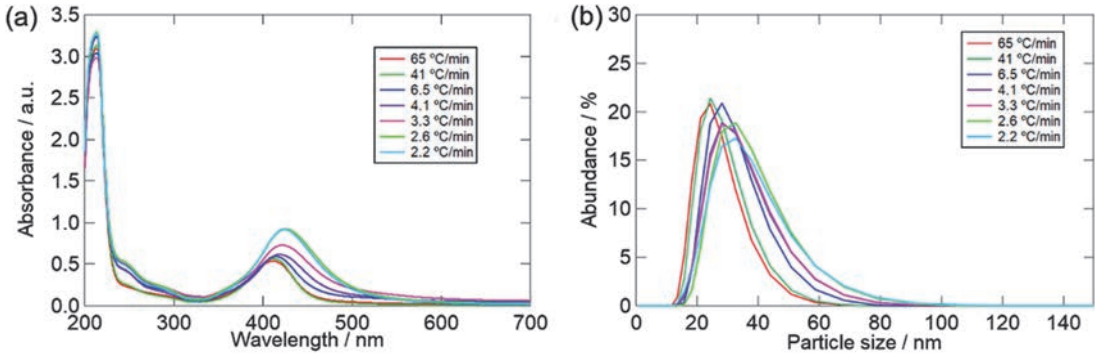

Figure 1. (a) UV − vis absorption spectra and (b) DLS size distribution of Ag NPs in ethylene glycol observed in synthesis under different heating rates.

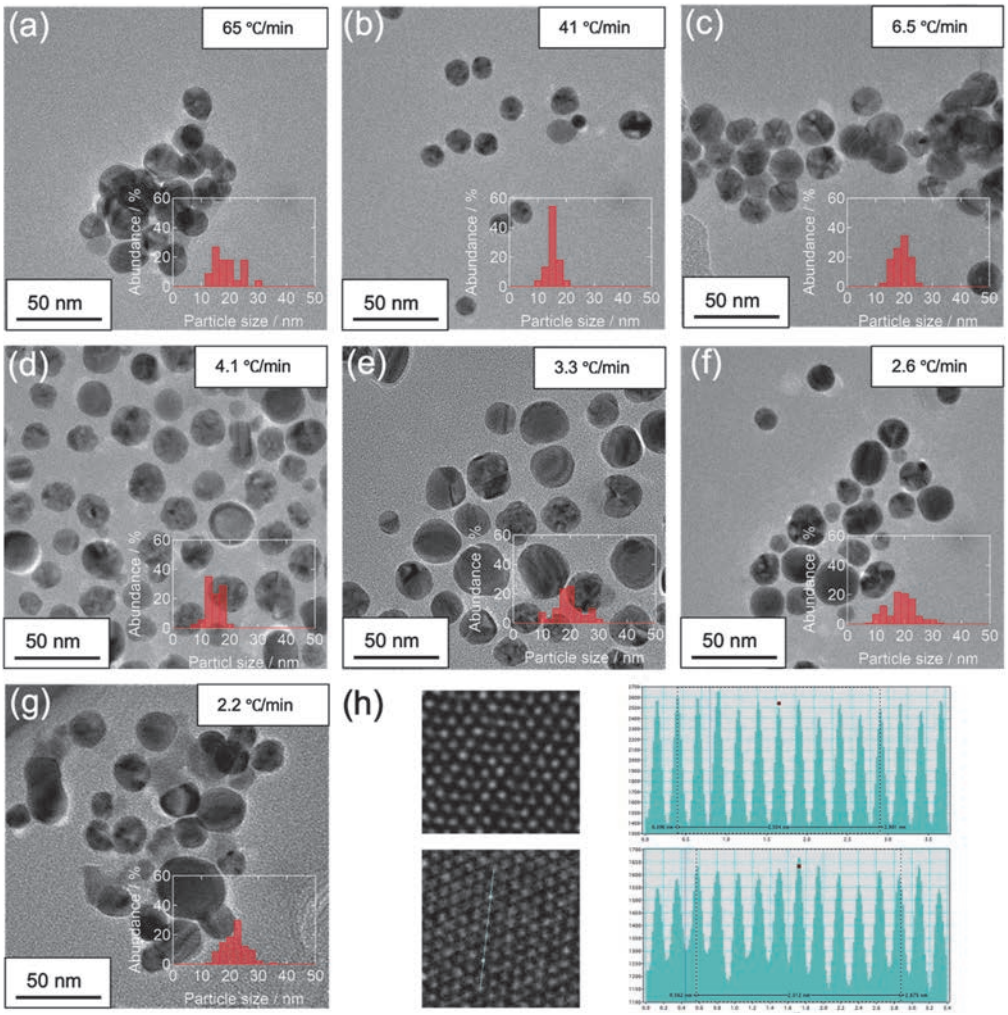

Figure 2. (a-g) HR-TEM images and histograms distribution of Ag NPs synthesized under different heating rates. (h) Left: Higher magnified view of the particles synthesized at heating rate of 65 ℃/min, demonstrating the crystalline structure of Ag NPs. Right: Line profile of the indicated area from left images.

between surface effects and internal energy.

The size distributions of synthesized Ag NPs were also compared to DLS measurements, as depicted in Figure 3. Notably, the size distributions derived from DLS measurements consistently exhibit a shift towards larger particles compared to those obtained from HR-TEM analysis. This discrepancy arises because HR-TEM analysis specifically evaluates the size of Ag NPs, whereas the DLS measurement, by principle, assess the hydrodynamic size of Ag NPs stabilized with PVP modified on their surface.

Figure 4(a) presents the crystal structure of Ag NPs

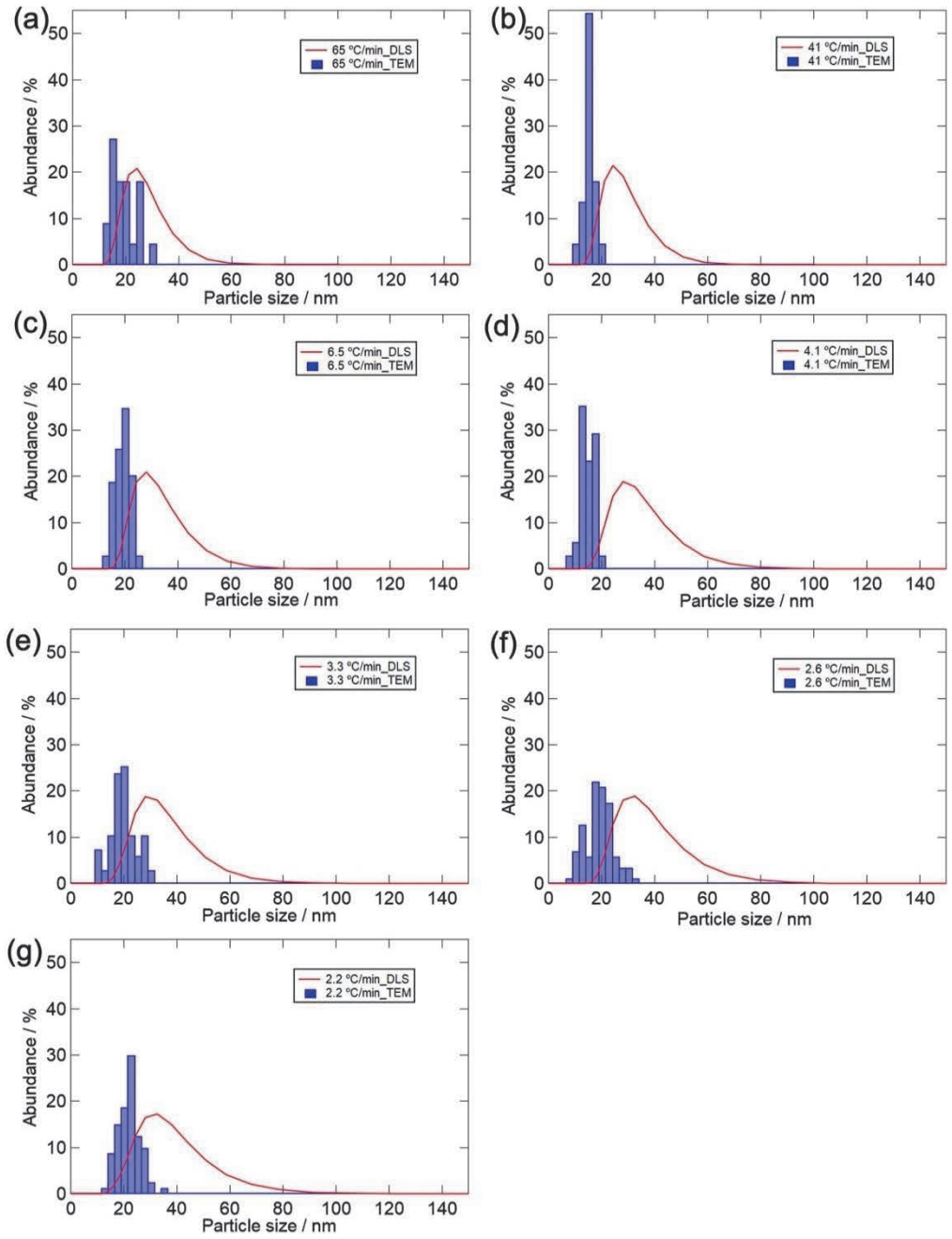

Figure 3. Comparison of Ag NPs particle size distribution obtained from HR-TEM images and from DLS measurements.

synthesized using microwave-assisted liquid-phase reduction method, as observed through HR-TEM. In contrast, the crystal structure identified by green squares in Figure 4(a) is discerned as a single crystal with an fcc structure through the FFT pattern, while those encircled by yellow squares represent a polycrystalline state with 4H/fcc. Figure 4(b) shows the ratio of single crystalline to polycrystalline Ag NPs synthesized at each temperature heating rate, based on the analysis of HR-TEM images. It highlights that Ag NPs synthesized under fast heating rate conditions exhibit a higher proportion of polycrystals, whereas the percentage of polycrystals decreases as the heating rate slows down in synthesis processes. Previously, it has been reported that Pt NPs synthesized under fast heating tend to be polycrystal with twinned crystal, and single crystalline Pt NPs obtained in microwave-assisted slow heating.[14] In this experiment, Ag NPs synthesized via microwave polyol reaction, the same method used for Pt NPs synthesis, predominantly displayed polycrystalline Ag NPs under faster heating rates, consistent with previous findings for Pt NPs. However, Ag NPs synthesized at slower heating rates still exhibited a notable presence of polycrystals, unlike the behavior observed with Pt NPs. This suggests that Ag NPs might be more inclined towards polycrystallization compared to Pt NPs. We

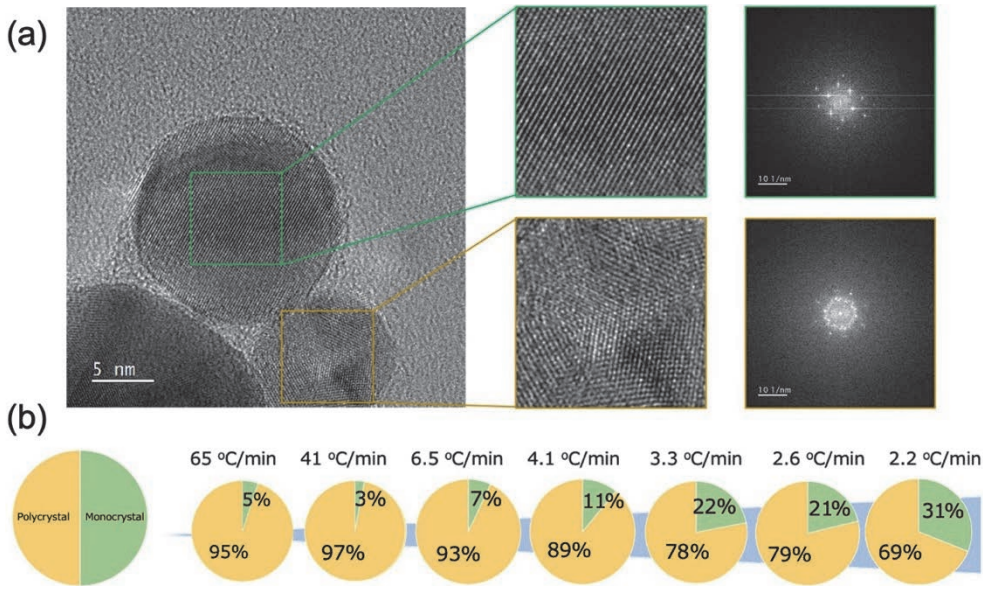

Figure 4. Single-crystalline and polycrystalline Ag NPs observed by HR-TEM (a) and the investigation of the proportion of single and polycrystalline Ag NPs synthesized at each microwave heating condition (b).

have previously reported that a new reaction pathway emerges in the polyol reaction when ethylene glycol is used. When ethylene glycol is heated, the reducing agent acetaldehyde is generated, and the acetaldehyde reacts with metal ions, and the metal ions are reduced to synthesize nanoparticles. However, in this reaction, the acetaldehyde further reacts to generate byproducts of diacetyl and acetaldehyde glycol acetal. Therefore, in order to further investigate the reaction mechanism, we performed GC-FID on the gas samples collected from the present system during polyol synthesis at a target temperature of 160 ℃ under gas flow. As shown in Figure 5(a), when the heating rate was slow, acetaldehyde existed stably, while when the heating rate was fast, a large amount of acetaldehyde glycol acetal that reacted with acetaldehyde was detected. It can be inferred that when the heating rate was slow, there was more reducing agent, and the reducing agent gradually supplied metal ions, and the metal ions were slowly reduced, thereby promoting the growth of single crystals in the 4H phase. When the heating rate was fast, the metal ions were quickly reduced, and fcc and 4H phases existed simultaneously in the polycrystalline nanoparticles. This is also consistent with the previous report that for Ag, the 4H phase requires slower growth kinetics compared to the fcc phase.[25, 32, 33]

Figure 5(b) depicts the zeta potential of Ag NPs synthesized by microwave-assisted fast (65 ℃/min) and slow (2.2 ℃/min) heating across a pH range of 7~9, and the zeta potential of solutions containing varying

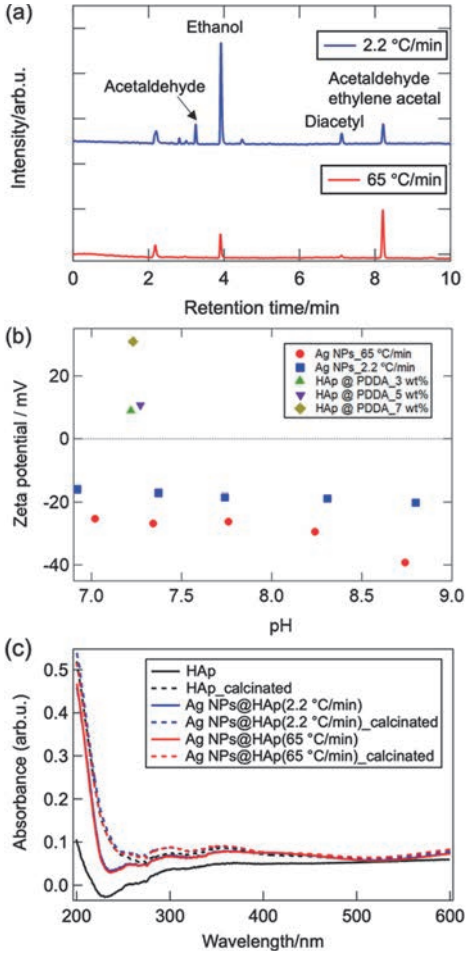

Figure 5. (a) GC-FID spectra of gases generated in the synthesis stage of Ag NPs through microwave-assisted fast heating and slow heating. (b) Zeta potential of Ag NPs and HAp with addition of PDDA. (c) UV–vis spectra of bare HAp and Ag NPs@HAp composites before and after calcination.

amounts of PDDA in HAp slurry. The Ag NPs exhibited a negatively charge within the pH range of 7~9, with the zeta potential decreased as the pH approached 9. This decrease was particularly pronounced for Ag NPs synthesized at a fast heating rate of 65 ℃/min. Additionally, based on the results of DLS and TEM observations, it was confirmed Ag NPs synthesized at a fast heating rate exhibited smaller particle size and better dispersibility. Considering the zeta potential values, it is inferred that Ag NPs synthesized at a fast heating rate promote the formation of a thick electric double layer, superior dispersibility. Consequently, it is unsurprising that the zeta potential values of Ag NPs synthesized at a heating rate of 65 ℃/min within the pH range of 7~9 surpass those of Ag NPs synthesized at a heating rate of 2.2 ℃/min. Furthermore, to facilitate the electrostatic adsorption of Ag NPs on HAp, PDDA was introduced to impart a positive charge to HAp slurry, aligning with the negative charge of Ag NPs. The exact loading amounts of Ag NPs on HAp were estimated by ICP-OES analysis to be 0.086 wt% and 0.093 wt% for fast and slow heating, respectively. After calcination, the UV–vis spectra was used to compare the optical properties of Ag NPs@HAp. As shown in Figure 5(c), no significant change was observed in the surface plasmon resonance peak at 400–420 nm, suggesting that the Ag nanoparticles largely retained their original size and morphology. Based on this, we infer that the structural features of the Ag NPs were preserved during calcination. Previous studies have shown that the 4H phase in Ag is a size-stabilized structure typically observed in nanocrystals with diameters below 30 nm.[29, 31, 34] In our present study, Ag NPs smaller than 30 nm are uniformly embedded within the HAp matrix, which may inhibit grain growth during calcination and suppress the irreversible 4H → fcc transformation. Notably, the hexagonal phase has been reported to revert to the cubic structure upon heating, mainly through thermally induced grain growth. Therefore, the nanoscale confinement and low Ag loading in HAp matrix may contribute to the potential retention of the 4H phase after calcination.

Figures 6(a-c) present the results of VOC decomposition of bare HAp and HAp loaded with Ag NPs synthesized in the microwave-assisted liquid-phase reduction method at a heating rate of 65 ℃/min and 2.2 ℃/min. The peaks observed at retention times of 2.1 min, 2.5 min, 2.9 min, and 7 min correspond to ethylene, acetaldehyde, ethanol, and ethyl acetate, respectively.[14] As we reported previously, the complete decomposition of ethylene acetate on HAp can be attributed to the generation of thermally activated radicals and specific acidic/basic sites on the HAp surface. It has been suggested that the super active radical-induced intermolecular cleavage of ethylene acetate and subsequent oxidation reaction corresponding to basic sites play a crucial role in CO_2 selectivity. Figure 6(d) depicts the conversion efficiency of ethylene acetate on different catalysts as a function of decomposition temperature. While bare HAp starts to decompose the ethylene acetate at a temperature higher than 200 ℃, the Ag NPs@HAp composites using a substantially low trace loading amount of Ag NPs (less than 0.1 wt %) show sufficient catalytic activity at a lower temperature.[35-38] The Ag NPs@HAp composites as well as bare HAp achieve almost 100% conversion efficiency at a temperature of 400 ℃. With respect to CO_2 product selectivity, as shown in Figure 6(e), the CO_2 selectivity at lower temperature (200 ℃) was up to 100% using the HAp loaded with Ag NPs synthesized via microwave-assisted fast heating. This may be due to the formation of a charge gradient at the interface between the fcc and 4H phases (e.g., electron transfer from the fcc phase to the 4H phase), which enhances the activation and migration ability of super oxygen radicals, thereby accelerating the oxidation of VOCs.

Conclusion

In this study, we demonstrated the successful synthesis Ag NPs with controlled crystal phases (fcc and 4H) through microwave-assisted polyol reduction by modulating heating rates. The slower heating rate facilitated the formation of larger Ag NPs dominated by the metastable 4H phase, whereas faster heating produced smaller polycrystalline Ag NPs with coexisting fcc and 4H structures. This phase selectivity was attributed to the interplay between precursor reduction dynamics and growth kinetics: slower heating allowed gradual reduction and stabilization of the metastable 4H phase, while rapid heating promoted simultaneous nucleation and growth, leading to polycrystalline structures. When loaded onto HAp, the synthesized Ag NPs exhibited remarkable catalytic activity for oxidative decomposition of VOC, even at trace amounts (0.1wt%). The Ag NPs@HAp composite prepared via fast heating achieved 100% CO_2 selectivity at 200 ℃, outperforming both bare HAp and slow-heated Ag NPs@HAp. This enhanced performance was ascribed to interfacial electronic effects between the coexisting fcc and 4H

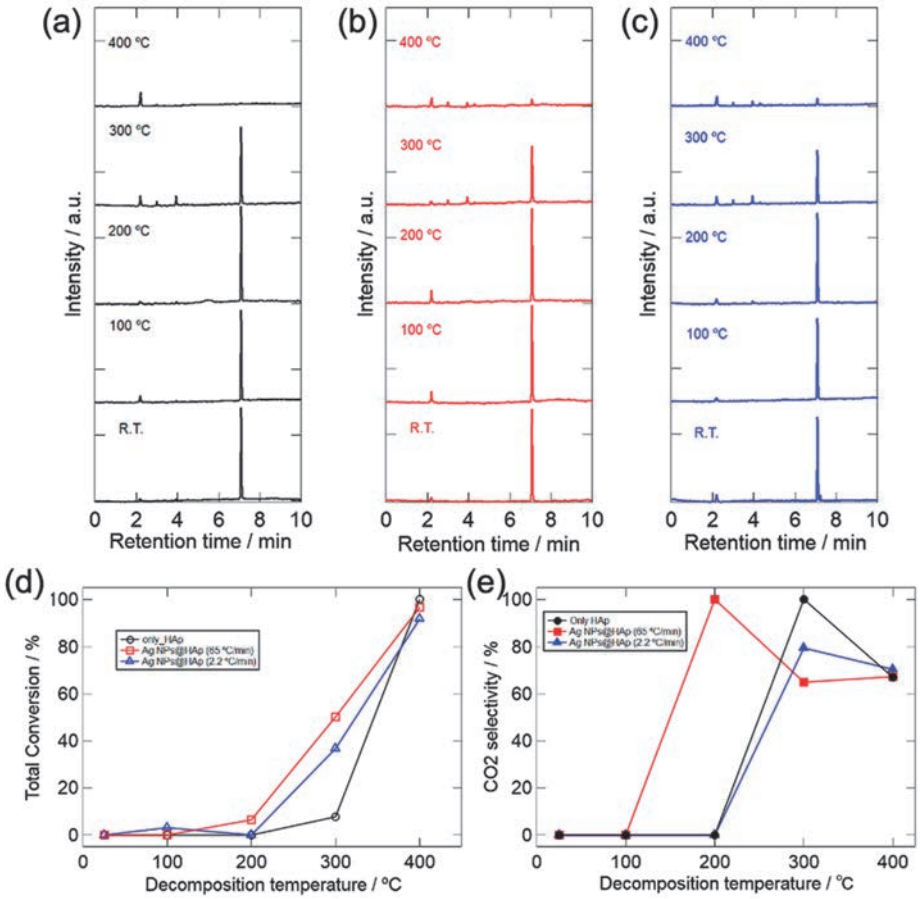

Figure 6. GC-FID spectra of decomposed gases collected before and after oxidative decomposition of ethyl acetate on HAp (a), Ag NPs @HAp composites by utilizing Ag NPs synthesized via microwave-assisted fast heating (b) and slow heating (c). (d)VOC conversion (e) CO_2 selectivity of ethyl acetate on bare HAp and Ag NPs@HAp catalysts obtained using Ag NPs synthesized via microwave-assisted heating.

phases, which likely promoted oxygen radical activation and facilitated VOC oxidation.

This work highlights the critical role of microwave heating dynamics in tailoring nanoparticle crystallinity and catalytic functionality. By bridging crystal phase engineering with environmental catalysis, our findings provide a scalable strategy for designing noble-metal catalysts with optimized activity and selectivity. Such efforts will further advance the development of energy-efficient catalysts for sustainable air purification technologies.

Acknowledgments

The author acknowledges Prof. Dr. Toru Asaka (Nagoya Institute of Technology) for HR-TEM observations.

References

[1] Ndolomingo M J, Bingwa N, Meijboom R. Review of supported metal nanoparticles: synthesis methodologies, advantages and application as catalysts[J]. Journal of Materials Science, 2020, 55(15): 6195-6241.

[2] Cui C H, Yu S H. Engineering interface and surface of noble metal nanoparticle nanotubes toward enhanced catalytic activity for fuel cell applications[J]. Accounts of chemical research, 2013, 46(7): 1427-1437.

[3] Klębowski B, Depciuch J, Parlińska-Wojtan M, et al. Applications of noble metal-based nanoparticles in medicine[J]. International journal of molecular sciences, 2018, 19(12): 4031.

[4] Samadi N, Hosseini S V, Fazeli A, et al. Synthesis and antimicrobial effects of silver nanoparticles produced by chemical reduction method[J]. DARU Journal of Pharmaceutical Sciences, 2010, 18(3): 168.

[5] Zhang J, Chaker M, Ma D. Pulsed laser ablationbased synthesis of colloidal metal nanoparticles for catalytic applications[J]. Journal of colloid and interface science, 2017, 489: 138-149.

[6] dos Santos H W L, Migowski P, Feil A F, et al. Sputtering deposition of nanoparticles onto liquid substrates: Recent advances and future trends[J]. Coordination Chemistry

Reviews (Print), 2013.

[7] Sakamoto M, Fujistuka M, Majima T. Light as a construction tool of metal nanoparticles: Synthesis and mechanism[J]. Journal of Photochemistry and Photobiology C: Photochemistry Reviews, 2009, 10(1): 33-56.

[8] Xia Y, Xia X, Peng H C. Shape-controlled synthesis of colloidal metal nanocrystals: thermodynamic versus kinetic products[J]. Journal of the American Chemical Society, 2015, 137(25): 7947-7966.

[9] Cushing B L, Kolesnichenko V L, O'connor C J. Recent advances in the liquid-phase syntheses of inorganic nanoparticles[J]. Chemical reviews, 2004, 104(9): 3893-3946.

[10] Xia Y, Gilroy K D, Peng H C, et al. Seed -mediated growth of colloidal metal nanocrystals[J]. Angewandte Chemie International Edition, 2017, 56(1): 60-95.

[11] Gerbec J A, Magana D, Washington A, et al. Microwave-enhanced reaction rates for nanoparticle synthesis[J]. Journal of the American Chemical Society, 2005, 127(45): 15791-15800.

[12] Lasri J, Charmier M A J, Haukka M, et al. Stereospecific synthesis of polysubstituted E-olefins by reaction of acyclic nitrones with free and platinum (II) coordinated organonitriles[J]. The Journal of Organic Chemistry, 2007, 72(3): 750-755.

[13] Dahal N, García S, Zhou J, et al. Beneficial effects of microwave-assisted heating versus conventional heating in noble metal nanoparticle synthesis[J]. ACS nano, 2012, 6(11): 9433-9446.

[14] Xin Y, Nagata T, Kato K, et al. Microwave-assisted synthesis of Pt nanoparticles via liquid-phase polyol reaction for catalytic volatile organic compound elimination[J]. ACS Applied Nano Materials, 2022, 5(3): 4305-4315.

[15] Fiévet F, Ammar-Merah S, Brayner R, et al. The polyol process: a unique method for easy access to metal nanoparticles with tailored sizes, shapes and compositions[J]. Chemical Society Reviews, 2018, 47(14): 5187-5233.

[16] Yue H, Zhao Y, Ma X, et al. Ethylene glycol: properties, synthesis, and applications[J]. Chemical Society Reviews, 2012, 41(11): 4218-4244.

[17] Nakamura S, Sato M, Sato Y, et al. Synthesis and application of silver nanoparticles (Ag NPs) for the prevention of infection in healthcare workers[J]. International journal of molecular sciences, 2019, 20(15): 3620.

[18] Akter M, Sikder M T, Rahman M M, et al. A systematic review on silver nanoparticles-induced cytotoxicity: Physicochemical properties and perspectives[J]. Journal of advanced research, 2018, 9: 1-16.

[19] Tan Z Q, Yin Y G, Guo X R, et al. Tracking the transformation of nanoparticulate and ionic silver at environmentally relevant concentration levels by hollow fiber flow field-flow fractionation coupled to ICPMS[J]. Environmental Science & Technology, 2017, 51(21): 12369-12376.

[20] Zhu Y J, Chen F. Microwave-assisted preparation of inorganic nanostructures in liquid phase[J]. Chemical reviews, 2014, 114(12): 6462-6555.

[21] Torras M, Roig A. From silver plates to spherical nanoparticles: snapshots of microwave-assisted polyol synthesis[J]. ACS omega, 2020, 5(11): 5731-5738.

[22] Dzido G, Jarzębski A B. Fabrication of silver nanoparticles in a continuous flow, low temperature microwave-assisted polyol process[J]. Journal of Nanoparticle Research, 2011, 13: 2533-2541.

[23] Ider M, Abderrafi K, Eddahbi A, et al. Rapid synthesis of silver nanoparticles by microwave-polyol method with the assistance of latex copolymer[J]. Journal of Cluster Science, 2017, 28: 1025-1040.

[24] B. G. Julio et. al, Journal of Applied Polymer Science. 11 (2007) 45-53.

[25] Cheng H, Yang N, Lu Q, et al. Syntheses and properties of metal nanomaterials with novel crystal phases[J]. Advanced Materials, 2018, 30(26): 1707189.

[26] Lu Q, Wang A L, Cheng H, et al. Synthesis of hierarchical 4H/fcc Ru nanotubes for highly efficient hydrogen evolution in alkaline media[J]. Small, 2018, 14(30): 1801090.

[27] Henglein A. Physicochemical properties of small metal particles in solution:" microelectrode" reactions, chemisorption, composite metal particles, and the atom-to-metal transition[J]. The Journal of Physical Chemistry, 1993, 97(21): 5457-5471.

[28] Dadosh T. Synthesis of uniform silver nanoparticles with a controllable size[J]. Materials letters, 2009, 63(26): 2236-2238.

[29] Taneja P, Banerjee R, Ayyub P, et al. Observation of a hexagonal (4 H) phase in nanocrystalline silver[J]. Physical review B, 2001, 64(3): 033405.

[30] Hinokuma S, Misumi S, Yoshida H, et al. Nanoparticle catalyst preparation using pulsed arc plasma deposition[J]. Catalysis Science & Technology, 2015, 5(9): 4249-4257.

[31] Liu X, Luo J, Zhu J. Size effect on the crystal structure of silver nanowires[J]. Nano letters, 2006, 6(3): 408-412.

[32] Liang C, Terabe K, Hasegawa T, et al. Formation of metastable silver nanowires of hexagonal structure and

their structural transformation under electron beam irradiation[J]. Japanese journal of applied physics, 2006, 45(7R): 6046.

[33] Singh A, Sai T P, Ghosh A. Electrochemical fabrication of ultralow noise metallic nanowires with hcp crystalline lattice[J]. Applied Physics Letters, 2008, 93(10).

[34] Chakraborty I, Shirodkar S N, Gohil S, et al. The nature of the structural phase transition from the hexagonal (4H) phase to the cubic (3C) phase of silver[J]. Journal of Physics: Condensed Matter, 2014, 26(11): 115405.

[35] Yang Y, Xu X, Sun K. A highly efficient copper supported catalyst for catalytic combustion of ethyl acetate[J]. Catalysis Communications, 2006, 7(10): 756-760.

[36] Xiao R, Qin R, Zhang C, et al. Catalytic decomposition of ethyl acetate over La-modified Cu–Mn oxide supported on honeycomb ceramic[J]. Journal of Rare Earths, 2021, 39(7): 817-825.

[37] Pearce J N, Ott C V. A study of the mechanism of the catalytic decomposition of ethyl acetate by nickel at various elevated temperatures[J]. The Journal of Physical Chemistry, 2002, 28(11): 1201-1210.

[38] Tsunashima M, Kitaori N. Decomposition of gaseous ethyl acetate with spherical pellets of Fe-Pt/Al_2O_3 catalyst using a combustion method[J]. Material technology, 2021, 39: 1-7.